HHS Public Access

Author manuscript

Conf Proc IEEE Eng Med Biol Soc. Author manuscript; available in PMC 2015 August 01.

Published in final edited form as:

Conf Proc IEEE Eng Med Biol Soc. 2014 ; 2014: 5101–5104. doi:10.1109/EMBC.2014.6944772.

Estimating Dense Cardiac 3D Motion Using Sparse 2D Tagged MRI Cross-sections*

Siamak Ardekani[1], **Geoffrey Gunter**[2], **Saurabh Jain**[3], **Robert G. Weiss**[4], **Michael I. Miller**[5], and **Laurent Younes**[6]

Siamak Ardekani: sardekani@jhu.edu; Geoffrey Gunter: gmg@cis.jhu.edu; Saurabh Jain: saurabh@cis.jhu.edu; Robert G. Weiss: rweiss@jhmi.edu; Michael I. Miller: mim@cis.jhu.edu; Laurent Younes: laurent.younes@jhu.edu

[1]The Center for Imaging Science, Johns Hopkins University, Baltimore, MD 21218, USA

[2]Department of Biomedical Engineering, Stony Brook University, Stony Brook, NY 11794, USA

[3]Center for Imaging Science, Johns Hopkins University, Baltimore, MD 21218, USA

[4]Department of Medicine, section of Cardiology, Johns Hopkins Medical Institutions, Baltimore, MD 21287, USA

[5]Center for Imaging Science, Johns Hopkins University, Baltimore, MD 21218, USA

[6]Center for Imaging Science, Johns Hopkins University, Baltimore, MD 21218, USA

Abstract

In this work, we describe a new method, an extension of the Large Deformation Diffeomorphic Metric Mapping to estimate three-dimensional deformation of tagged Magnetic Resonance Imaging Data. Our approach relies on performing non-rigid registration of tag planes that were constructed from set of initial reference short axis tag grids to a set of deformed tag curves. We validated our algorithm using *in-vivo* tagged images of normal mice. The mapping allows us to compute root mean square distance error between simulated tag curves in a set of long axis image planes and the acquired tag curves in the same plane. Average RMS error was 0.31±0.36(SD) mm, which is approximately 2.5 voxels, indicating good matching accuracy.

I. INTRODUCTION

Tagged magnetic resonance imaging (MRI) is a well established technique to characterize the regional motion of the myocardium [1], [2]. In tagging, a selective magnetic presaturation plane is generated that is perpendicular to the image acquisition plane creating dark bands that move along with the tissue during myocardial contraction and relaxation phases. Typically, two sets of perpendicular tag planes are used to create two sets of parallel bands (tag grid) that are perpendicular to each other at an initial undeformed time point in the cardiac phase. Characterizing regional myocardial contractility using tagged MRI relies on tracking adjacent tag intersection points to identify a relative increase or decrease in their distance from one cardiac phase to another. Several post-processing techniques have been

*This work was supported by funding from the National Institute of Health: R21HL109968, R24HL085343, and R01HL063030.

developed to facilitate extracting tag displacements over different cardiac phases [3], [4]. These techniques have used a variety of approaches including but not limited to active contour models [5], [6], [7], optical flow [8], [9], harmonic phase [10], and non-rigid registration [11], [12]. While each of these methods presents with its own advantages and disadvantages [3], a recent study has indicated that non-rigid registration algorithms outperform other methods in tracking tag curves, particularly when dealing with lower-quality image data [13].

Given that the tag data are usually collected using a few planes, the challenge is to construct a dense 3D deformation field from tag planes to enable an accurate estimation of myocardial contractility. Several groups have used non-rigid registration techniques based on splines and information-theoretic similarity measures to perform volumetric analysis of tagged MRI data [11], [12], [14]. In this work we use Large Deformation Diffeomorphic Metric Mapping (LDDMM) to perform non-rigid transformation of tag planes reconstructed from non-deformed tag lines at end diastole (ED) to a set of tag curves at a later time point in the cardiac cycle. Representing a stack of contiguous tag lines with tag planes reflects the physical reality of MRI tagging. Tag lines (at an initial cardiac phase) and curves (at a later cardiac phase) are representations of the intersection of nondeformed and deformed tag planes with the fixed image planes (Ex. short axis planes) in the 3D space, respectively. LDDMM generates diffeomorphic (smooth and invertible) dense 3D transformations that map tag planes to tag curves avoiding any fusion or tear when deforming the planes. Additionally, LDDMM, by design, is able to accommodate large non-linear motion which is suitable for myocardial motion analysis. We used our algorithm to estimate dense 3D cardiac motion using *in-vivo* short axis tag images collected from normal mice and validated our results against the tag data collected along the long axis planes in the same animal.

II. METHODS

A. Imaging Protocol

In-vivo heart images of 4 adult male wild type sham mice were acquired using Bruker NMR/MRI spectrometer equipped with a 11.7T magnet and a gradient set capable of developing gradient strengths of 740mT/m (Bruker Biospin, Germany). The mice were positioned on the MRI detector coil and an MRI gating trigger was established via ECG leads and respirator pillow was used. SPAMM tagged MRI was collected (15 frames, echo time (TE) = 1.4 ms, repetition time (TR) = 8 ms, slice thickness = 1 mm, In plane resolution was $0.130 \times 0.130\ mm^2$, flip angle = 10°, NEX = 7, tag spacing = 0.2 mm, tag distance = 0.75 mm) at both short (6–8 slices) and long axis (3 slices) which resulted in short axis (SAX) and long axis (LAX) images that contained orthogonally oriented tags. The animal protocol was approved by the Institutional Animal Care and Use Committee of the Johns Hopkins University. Epicardial and endocardial contours were isolated using a semi-automatic freely available software called Segment [15](http://medviso.com/products/segment/).

B. Preprocessing

Tag lines in short and long axis planes were tracked using an approach that was described previously in [16]. Briefly, tag lines were manually traced at a baseline, non-deformed cardiac phase (ED) for each short and long axis image planes separately. Tag lines were then traced over different cardiac phases by performing a 2D based non-rigid intensity matching using LDDMM [17]. Locations of tag lines at any particular slice and cardiac phase were manually corrected, if necessary, using ImageJ software tool [18]. The coordinates of points that constitutes each tag curve were transformed from the image coordinate system to the scanner coordinate system using Matlab® (Mathworks Inc.), exploiting the information that has been stored in the header of original DICOM tagged image files. This ensures that the spatial correlation between short and long axis image planes is maintained, which enables us to perform a validation study of 3D motion estimation. Once in the scanner coordinate system, the short and long axis tag lines were rotated to align the long axis of left ventricle with the *z*-axis. Next a set of parallel tag planes were fitted to the contiguous stack of tag lines that was collected at ED (Fig. 1 left). Each plane was then mapped to the separate stack of tag curves (Fig. 1 right) that was collected at end-systole (ES) using the method that is described in section II-C. The energy function for mapping the tag planes was optimized using the information from all tag planes generated from SAX images.

C. Matching Planes to Curves

In this section, we describe the non rigid deformation used to match the tag planes to the tag curves. More generally, given a surface S and a collection of planar curves $\Gamma = \gamma_1, \ldots, \gamma_n$, we would like to find an optimum transformation that maps the template surface S to the curves.

As mentioned in the introduction, we use LDDMM [17] (chap. 11) for the matching, which enables large deformations while avoiding tears and fusions of the tag planes. In this setting a deformation φ^v is obtained via integration of a time varying vector field v,

$$\partial_t \phi_t^v = v_t \circ \phi_t^v$$

and minimizing the following cost functional over v in an appropriate Hilbert Space V,

$$E(v) = \int_0^1 \|v_t\|_V^2 \, dt + D(\phi_1^v(S), \Gamma) \quad (1)$$

The first term in the functional controls the norm of the vector field v, which, in turn, controls the smoothness of the diffeomorphism φ^v, and the second penalizes the mismatch between the mapped surface and the curves. The Hilbert space V is chosen to be a Reproducing Kernel Hilbert Space (RKHS) [17] (chap. 9), with kernel $K(x, y) = g(\|x - y\|)Id_{\mathbb{R}^3}$, where $g(t) = \exp(\frac{-t^2}{2\sigma^2})$, for a parameter σ. The details of the algorithm as it applies to surface matching can be found in [19]. The surface evolution for our work follows [19], but now the mismatch must be defined between a surface and a set of curves rather than between two surfaces. We describe this mismatch term next.

Without loss of generality, let us assume that all curves are in parallel planes, and that these planes are horizontal, with respective equations $z = \lambda_k$ for $\lambda_1, \ldots, \lambda_n \in \mathbb{R}$. We assume that the curves are oriented and represented as vector measures [20]. To simplify the discussion, let us also assume that there is only one curve per plane. Denoting the unit normal to the curve γ_k in the plane $z = \lambda_k$ by n_k, we define the vector measure associated to γ_k by

$$(\gamma_k|w) = \int_{\gamma_k} w \cdot n_k$$

where w is a 3D vector field, and $\int_{\gamma_k}$ denotes the line integral over γ_k.

Let $S_\lambda = S \cap [z = \lambda]$. This set is, in general, either empty, or a collection of curves, that can be oriented based on the orientation on S. More precisely, letting N denote the normal to S, we orient the normal, ν_λ, to S_λ so that $\nu_\lambda \cdot N > 0$. The only situation in which this is not defined is when ν_λ is perpendicular to N, in which case $z = \lambda$ is tangent to S and the intersection is degenerate.

Since S_λ can also be considered as a vector measure, we can define the cost function

$$D(S, \Gamma) = \sum_{k=1}^{n} \|S_{\lambda_k} - \gamma_k\|_W^2 \quad (2)$$

where $|\cdot|_W$ is the kernel-based norm between vector measures representing plane curves [20].

Written as such, this cost function is not tractable, since it will be minimized with respect to S and its evaluation requires computing intersections between the surface and the planes of interest (which are fixed). We may however obtain something feasible if we represent the set S_λ using Dirac-δ functions.

For this purpose, let H_ε be a smooth approximation of the Heaviside function, such that $\lim_{\varepsilon \to 0} H_\varepsilon = H_0 = \mathbf{1}_{[0,+\infty)}$. Let $\delta_\varepsilon = H_\varepsilon'$. Then, we can make the approximation

$$(S_\lambda|w) \simeq \int_S \delta_\varepsilon(z(m) - \lambda) w(m) \cdot \nu_z(m) \rho(m) ds(m) \quad (3)$$

where σ is the area form on S, $z(m)$ is the z-coordinate of the point m on the surface, and $\rho(m)$ is the cosine of the angle between N and the horizontal plane (i.e., $\sqrt{1 - N_z^2}$). This choice is justified since the integral in (3) converges to the line integral over S_λ, as ε goes to 0 (see Appendix).

Note that $\rho \nu_z$ is the same as the horizontal projection of the normal to S on the horizontal plane. Letting $\tilde{N}$ denote this projection, we can rewrite (3) as

$$(S_\lambda|w) \simeq \int_S \delta_\varepsilon(z(m)-\lambda)w(m)\cdot\tilde{N}(m)ds(m) \quad (4)$$

When S is triangulated, with F_S denoting the set of faces, the resulting vector measure is discretized as

$$(S_\lambda|w)=\sum_{f\in F_S}\delta_\varepsilon(z(c(f))-\lambda)w(c(f))\cdot\tilde{N}_a(f)$$

where $\tilde{N}_a(f)$ is the projection of the normal to the face f weighted by its area onto the horizontal plane, and $c(f)$ is the center of f. The norm between vector measures in (2) associated to a kernel ξ is then computed using the following formula for the inner product between S_λ and γ_k,

$$<S_\lambda,\gamma_k>=\sum_{f,j}\xi(c(f),\gamma_{k,j})\delta_\varepsilon(z(c(f))-\lambda)\tilde{N}_a(f)\cdot\tilde{n}_{k,j}$$

where γ_k is discretized as ($\gamma_{k,1}$, …, $\gamma_{k,q}$) and $\tilde{n}_{k,j}$ is the length-weighted normal.

The generalization of this approximation to planes other than the horizontal plane is straightforward. If η is a unit vector, and the plane under consideration has equation $\eta\cdot m = \lambda$, replace $z(m)$ by $\eta\cdot m$ and $\tilde{N}_a$ by the projection of N_a, on the plane perpendicular to η, i.e., $\tilde{N}_a = N_a - (N_a\cdot\eta)\eta$.

D. Validation

We evaluated the accuracy of our algorithm to estimate 3D tag deformation by first mapping ED tag planes that were perpendicular to the SAX image planes to the corresponding stack of SAX tag curves extracted at ES. This process generated a dense 3D deformation field that could be applied to any arbitrary tag plane. Along with SAX image planes, we also acquired 3 LAX image planes that were angled at 60° relative to each other. Each LAX image plane contained 2 sets of horizontal (8–10) and vertical (8–10) tag curves constructed from the set of tag planes that were perpendicular to each LAX image plane. We applied the deformation map from ED to ES, which was estimated from SAX tag curves, to the LAX tag planes. This generated a set of deformed LAX tag surfaces. The intersection of these deformed LAX tag planes with the original LAX image plane generates a new set of tag curves that should ideally coincide with the acquired LAX tag curves (Fig. 2). Any deviation between original and estimated LAX tag curves represents inaccuracy of 3D tag deformation estimation. We characterized this deviation by calculating the root mean square (RMS) distance error between the acquired and estimated LAX tag curves.

III. RESULTS

The performance of our matching algorithm in mappping ED tag planes to the corresponding stack of contiguous SAX tag curves at ES is illustrated in Fig. 3. Visual

inspection of the mapping indicates good performance of our algorithm to accommodate large deformation of tag curves. Note that the pattern of deformation is heterogeneous across myocardium, therefore, non-rigid matching appears to be an appropriate approach to characterize myocardial contractility.

Results of quantitative assessment of our algorithm have been summarized in table I. These initial results indicate that our algorithm is able to estimate large deformation with average error of approximately 2.5 voxels (in plane resolution was 0.130 × 0.130 mm). Note that we have estimated myocardial deformation solely from the short axis images, and used the long axis images to validate the results. Furthermore, note that we have applied our algorithm on a small size animal model. Due to small scale of mouse heart, the number and length of tag curves are typically few and short, respectively. Therefore accurate estimation of dense 3D myocardial deformation become extremely challenging, but our algorithm is still able to perform well.

IV. CONCLUSIONS

We presented and validated an estimation of 3D dense deformation of left ventricular myocardium using LDDMM algorithm. In this method we employed information encoded in SAX tagged MRI to construct detailed spatial displacement of tag planes during ventricular contraction which was validated by the information from LAX tagged MRI. However, both SAX and LAX tagged MRI can be combined to derive the registration process. This method can be readily applied to all cardiac phases to construct Lagrangian strain tensors. While we used tag planes as an initial reference point, our method would allow using non-planar surfaces as a reference point, which would be suitable for the circumstances when initial tag data have been collected after ventricular contraction has already started.

Acknowledgments

S. A. thanks Mrs. Michelle Leppo for her assistance with animal preparation and Dr. Jiadi Xu for his assistance with image acquisition.

References

1. Zerhouni EA, Parish DM, Rogers WJ, Yang A, Shapiro EP. Human heart tagging with MR imaging: a method for noninvasive assessment of myocardial motion. Radiology. 1988; 169:59–63. [PubMed: 3420283]
2. Axel L, Dougherty L. MR imaging of motion with spatial modulation of magnetization. Radiology. Jun; 1989 171(3):841–5. [PubMed: 2717762]
3. Ibrahim, el-SH. Myocardial tagging by cardiovascular magnetic resonance: evolution of techniques–pulse sequences, analysis algorithms, and applications. J Cardiovasc Magn Reson. 2011; 13:36. [PubMed: 21798021]
4. Frangi AF, Niessen WJ, Viergever MA. Three-dimensional modeling for functional analysis of cardiac images: A review. IEEE Trans Med Imag. Jan.2001 20:225.
5. Guttman MA, Prince JL, McVeigh ER. Tag and contour detection in tagged MR images of teh left ventricle. IEEE Trans Med Imaging. 1994; 13:74–88. [PubMed: 18218485]
6. Amini AA, Chen Y, Curwen RW, Mani V, Sun J. Coupled B-snake grids and constrained thin-plate splines for analysis of 2-D tissue deformations from tagged MRI. IEEE Trans Med Imaging. 1998; 17:344–356. [PubMed: 9735898]

7. Tustison NJ, Davila-Roman VG, Amini AA. Myocardial kinematics from tagged MRI based on a 4-D B-spline model. IEEE Trans Biomed Eng. 2003; 50:1038–1040. [PubMed: 12892332]
8. Prince JL, McVeigh ER. Motion estimation from tagged MR image sequences. IEEE Trans Med Imaging. 1992; 11(2):238249.
9. Carranza-Herrezuelo N, Bajo A, Sroubek F, Santamarta C, Cristobal G, Santos A, Ledesma-Carbayo MJ. Motion estimation of tagged cardiac magnetic resonance images using variational techniques. Comput Med Imaging Graph. 2010; 34:514522.
10. Osman NF, Kerwin WS, McVeigh ER, Prince JL. Cardiac motion tracking using CINE harmonic phase (HARP) magnetic resonance imaging. Magn Reson Med. 1999; 42:10481060.
11. Chandrashekara R, Mohiaddin RH, Rueckert D. Analysis of 3-D myocardial motion in tagged MR images using nonrigid image registration. IEEE Trans Med Imaging. Oct; 2004 23(10):1245–50. [PubMed: 15493692]
12. Shi W, Zhuang X, Wang H, Duckett S, Luong DV, Tobon-Gomez C, Tung K, Edwards PJ, Rhode KS, Razavi RS, Ourselin S, Rueckert D. A comprehensive cardiac motion estimation framework using both untagged and 3-D tagged MR images based on nonrigid registration. IEEE Trans Med Imaging. Jun; 2012 31(6):1263–75. [PubMed: 22345530]
13. Smal, I.; Carranza-Herrezuelo, N.; Klein, S.; Niessen, W.; Meijering, E. Quantitative comparison of tracking methods for motion analysis in tagged MRI. Biomedical Imaging: From Nano to Macro, 2011 IEEE International Symposium on; 2011. p. 345-348.
14. Rougon N, Petitjean C, Preteux F, Cluzel P, Grenier P. A non-rigid registration approach for quantifying myocardial contraction in tagged mri using generalized information measures. Medical Image Analysis. 2005; 9(4):353375.
15. Heiberg E, Sjgren J, Ugander M, Carlsson M, Engblom H, Arheden H. Design and Validation of Segment a Freely Available Software for Cardiovascular Image Analysis. BMC Medical Imaging. 2010; 10(1)
16. Kotamraju, V.; McVeigh, E.; Beg, MF. Estimation of 3D myocardial motion from tagged MRI using LDDMM. Proc. SPIE 6511, Medical Imaging 2007: Physiology, Function, and Structure from Medical Images, 65112H; March 29, 2007;
17. Younes, L. Shapes and Diffeomorphisms. Vol. 11. New York: Springer-Verlag; 2010.
18. Schneider CA, Rasband WS, Eliceiri KW. NIH Image to ImageJ: 25 years of image analysis. Nature Methods. 2012; 9:671–675. [PubMed: 22930834]
19. Vaillant M, Glaunes J. Surface Matching via Currents. Information Processing in Medical Imaging. 2005; 19:381–392. [PubMed: 17354711]
20. Glaunes J, Qiu A, Miller MI, Younes L. Large Deformation Diffeomorphic Metric Curve Mapping. International Journal on Computer Vision. Dec.2008 80:317–336.

APPENDIX

To justify (3), assume a local chart $(u, v) \mapsto m(u, v)$ around the altitude λ such that

- **i.** $m(u, 0)$ coincides with S_λ
- **ii.** $m(u, v) - m(u, 0)$ is perpendicular to $\dot{m}_u(u, 0)$ and $v = z(m) - \lambda$ (taking $v \mapsto m(u, v)$ to be the curve given by the intersection between S and the plane passing by $m(u, 0)$ and perpendicular to $\dot{m}_u(u, 0)$). This implies, in particular, that $\dot{m}_u(u, 0) \cdot \dot{m}_v(u, 0) = 0$.

Then, if ω is a function on S which is supported by the chart, and letting $z(m)$ denote the altitude (third coordinate),

$$\begin{aligned}&\int_S \omega(m)\delta_\varepsilon(z(m)\\&\quad -\lambda)w(m)\\&\quad \cdot \nu_\lambda(m)\rho(m)d\sigma(m)\\&=\int\int \delta_\varepsilon(v)\omega(m(u,v))\rho(m(u,v))w(m(u,v))\\&\quad \cdot \nu_{v+\lambda}(m(u,v))|\dot{m}_u \times \dot{m}_v|dudv\end{aligned}$$

which converges, when $\varepsilon \to 0$, to

$$\int \rho(m(u,0))w(m(u,0)) \cdot \nu_\lambda(m(u,0))|\dot{m}_u(u,0)|\,|\dot{m}_v(u,0)|du$$

Now, since $z(m(u, v)) = v - \lambda$, we have $\nabla z(m) \cdot \dot{m}_v = 1$ and letting $b(m)$ be a unit tangent to S perpendicular to the tangent to S_λ, we find $|\dot{m}_v| = 1/|\nabla z(m) \cdot b(m)|$. But $|\nabla z(m) \cdot b(m)| = \rho(m)$, which therefore simplifies in the integral, and what remains is just the line integral along S_λ.

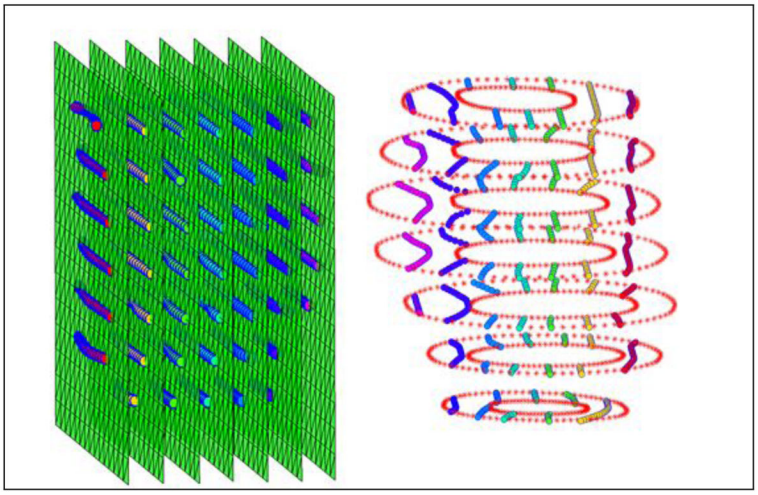

Fig. 1.

Left: An example of fitted tag planes to several stacks of left ventricular tag lines (colored circles) at ED. Right: An example of stack of tag curves at ES. Colors are assigned arbitrarily to highlight different stacks of tag lines/curves. For clarity, we have only shown part of the tag grid.

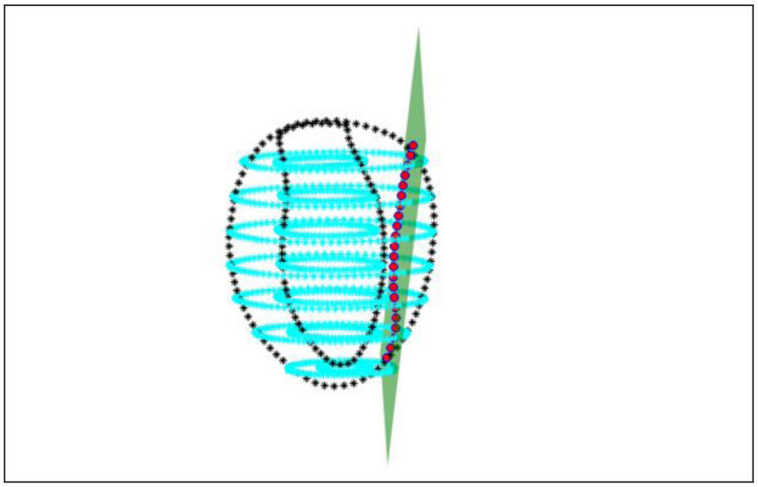

Fig. 2.

Schematic diagram of a sample LAX tag plane (green) at ED. As a result of myocardial contraction this plane deforms (not shown) and intersection of the deformed plane with the LAX image plane (black asterisks) will generate a new tag curve (red circles). Endo and epicardial contours extracted from SAX image planes are illustrated by cyan asterisks.

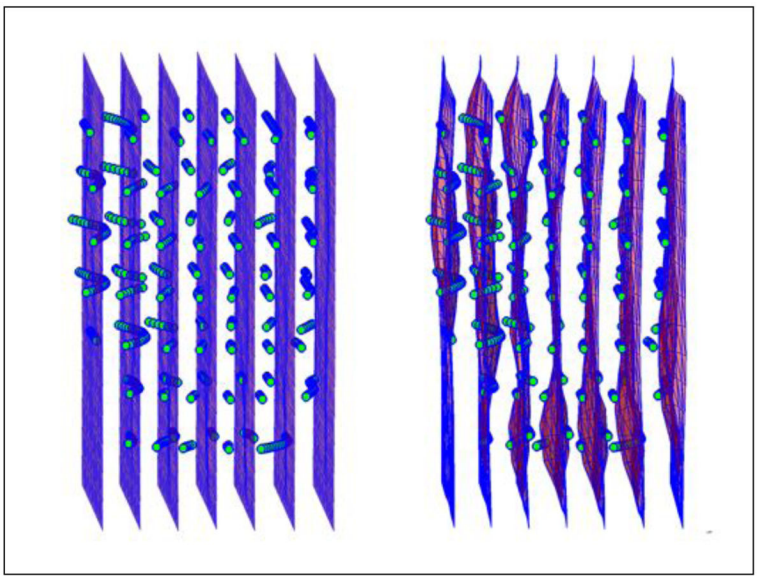

Fig. 3.

Example of tag plane-to-curve matching. Left: ED tag planes (purple) super-imposed on stack of tag curves (green circles) that was extracted at ES. Right: Deformed tag surfaces (red) after matching tag planes to the corresponding tag curve stacks (green circles). Note matching was conducted simultaneously for all planes.

TABLE I

RMS distance error (mm)

Animal	1	2	3	4
Mean(SD)	0.26(±0.30)	0.26(±0.26)	0.35(±0.31)	0.35(±0.53)